Measurement of sheared flows in the edge plasma of the CASTOR tokamak

Article *in* Plasma Physics Reports · November 2009
DOI: 10.1134/S1063780X09110087

7 authors, including:

Jana Brotánková
Czech Technical University in Prague

J. Stockel
The Czech Academy of Sciences

J. Horacek
The Czech Academy of Sciences

I. Duran
The Czech Academy of Sciences

ISSN 1063-780X, Plasma Physics Reports, 2009, Vol. 35, No. 11, pp. 980–986. © Pleiades Publishing, Ltd., 2009.
Published in Russian in Fizika Plazmy, 2009, Vol. 35, No. 11, pp. 1059–1065.

SMALL FUSION DEVICES

Measurement of Sheared Flows in the Edge Plasma of the CASTOR Tokamak[1]

J. Brotankova[a, b], J. Stockel[a], J. Horacek[b], J. Seidl[a], I. Duran[a], M. Hron[a], and G. Van Oost[c]

[a] *Institute of Plasma Physics AS CR, v.v.i., Association EURATOM/IPP.CR, Za Slovankou 3, 182 00 Praha 8, Czech Republic*

[b] *Faculty of Mathematics and Physics, Charles University in Prague, Praha, Czech Republic*

[c] *Department of Applied Physics, Ghent University, Gent, Belgium*

Received December 10, 2008; in final form, March 31, 2009

Abstract—The ion saturation current and floating potential are measured with high temporal (1 μs) and spatial (2.5 mm) resolutions at the plasma edge of the CASTOR tokamak by two poloidally spaced radial arrays of Langmuir probes. The radial electric field and the phase velocity of plasma fluctuations are estimated. The position of the velocity shear layer (VSL) is localized with a high precision. The shearing rate $\omega_{\mathbf{E}\times\mathbf{B}}$ determined and found to be comparable with the inverse of the correlation time of fluctuations $1/\tau_{ac}$ outside the VSL and about five times higher in the proximity of the VSL. A small impact of the shear on fluctuation level at the VSL is observed also in the statistic parameters of the U_{fl} and I_{sat}.

PACS numbers: 52.55.Fa, 52.70.-m

DOI: 10.1134/S1063780X09110087

1. INTRODUCTION AND EXPERIMENTAL SETUP

Understanding of plasma turbulence in magnetic confinement devices is believed to be one of the key elements leading to practical exploitation of fusion as an ultimate energy source for mankind. Turbulence is responsible for anomalously high losses of particles and energy at the plasma edge. In order to suppress the negative effects caused by turbulence, proper understanding of the phenomena occurring in the edge plasma region is necessary.

The shear of poloidal velocity is one of the mechanisms reducing turbulence at the plasma edge [1]. Natural shear occurs in magnetic fusion devices, created by turbulence, which is driven by an interchange instability from the low-field side [2]. Interplay between the velocity shear and the turbulence keeps the system near marginal stability [3]. If the shear exceeds a certain value, the turbulent structures are dissipated and a so-called transport barrier arises, consequently the plasma confinement is improved.

The shear of the poloidal velocity and of the radial electric field is measured in the edge plasma region of the CASTOR tokamak by means of Langmuir probes arrays. At first, let us describe certain specific features of CASTOR.

CASTOR is a tokamak with poloidal limiter (R = 40 cm, a = 8.5 cm, B_{tor} = 1.3 T, and I_p = 10 kA). The plasma column is typically shifted downward, as is schematically shown in Fig. 1. We can distinguish two regions, where magnetic field lines are open: the lim-

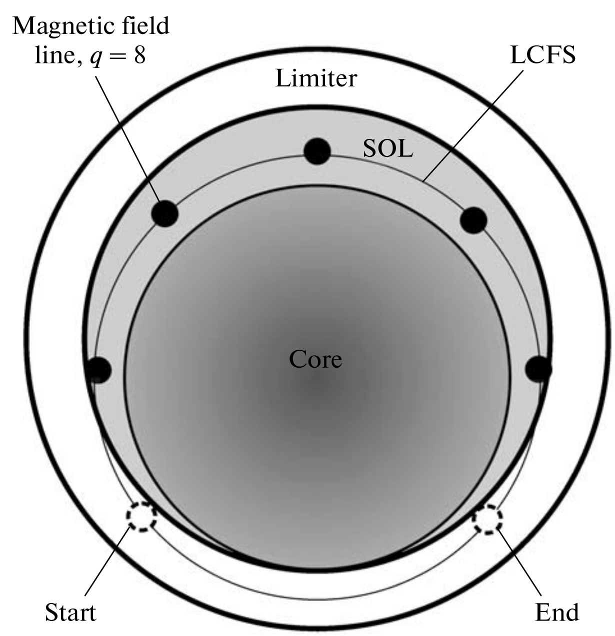

Fig. 1. Poloidal cross section of the CASTOR tokamak (vertical shift of the plasma).

[1] The article is published in the original.

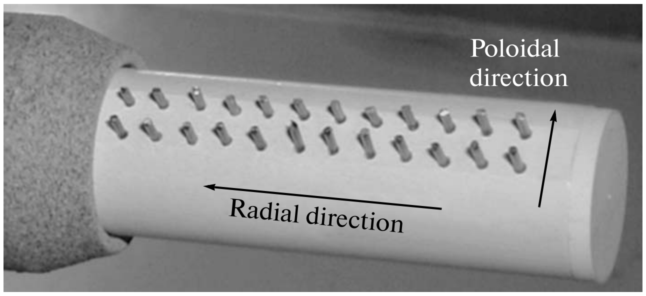

Fig. 2. Double rake probe.

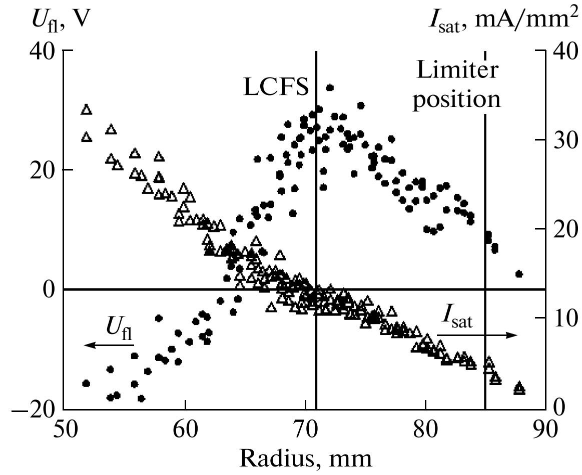

Fig. 3. Radial profile of the floating potential (circles) and the ion saturation current (triangles). The vertical lines show the position of the LCFS and the limiter [4].

iter shadow (the white area in the figure) and the light grey part labelled as the scrape off layer (SOL). In the shadow of the limiter, a particle needs one toroidal turn along the chamber to hit the limiter surface. A completely different situation occurs in the region labelled as SOL in the figure: The magnetic field lines cross the poloidal cross section several times before ending at the limiter. This setup is similar to a configuration with a toroidal limiter. The number of toroidal turns necessary for a magnetic field line to fully encircle the poloidal cross section of the torus is called safety factor q. For the edge plasma of the CASTOR tokamak, $q \approx 8$.

The edge plasma parameters are measured by a double rake probe, shown in Fig. 2, which consists of two radial arrays of 12 Langmuir probe tips each. The tips are made of molybdenum, spaced by 2.5 mm in poloidal as well as in radial direction. The probe is immersed into the plasma from the top of the tokamak chamber. The individual tips of the double rake probe measure either the floating potential U_{fl} or the ion saturation current I_{sat} with a temporal resolution of 1 μs.

2. RADIAL PROFILES AT THE PLASMA EDGE

Radial profiles of floating potential and ion saturation current (which is proportional to the plasma density), measured at the top of the CASTOR torus, are shown in Fig. 3 [4]. The maximum of the floating potential roughly corresponds to the radial position of the last closed flux surface (LCFS) [5].

The radial electric field E_{rad} is derived as $E_{rad} = -d\phi/dr$, where $\phi = U_{fl} + 2.5T_e$ is the plasma potential and T_e is the electron temperature. The electron temperature is not measured during these experiments; a radial profile from a set of discharges with similar regime was used [6, 7]. The typical value of the electron temperature gradient is ≈1 eV/mm in the ohmic discharges. The absolute value of the gradient of the floating potential is approximately 1.9 V/mm for $53 < r < 64$ mm, 4.0 V/mm for $64 < r < 70$ mm, and 1.7 V/mm for $71 < r < 87$ mm (see Fig. 3). The gradient of the floating potential changes its sign at LCFS being negative in the SOL and positive in the confinement region, as is further seen from Fig. 3. As a result, the radial electric field is positive in the SOL, while it takes negative values inside the LCFS. This electric field, in combination with the strong toroidal magnetic field B_{tor}, causes an $\mathbf{E}_{rad} \times \mathbf{B}_{tor}$ rotation in the poloidal direction. The poloidal rotation thus should have an opposite sign outside and inside the LCFS. Therefore, the position of the LCFS is sometimes labelled as the velocity shear layer (VSL).

3. DETERMINATION OF THE POLOIDAL PHASE VELOCITY OF PLASMA FLUCTUATIONS

The plasma flow velocity is not directly measured in this experiment. Instead, we determine the poloidal phase velocity of plasma fluctuations v_{ph} using two poloidally spaced Langmuir probes, it means in the lab frame. In principal, the phase velocity of the turbulence with respect to the ambient rotating plasma may be non-zero, however, previous studies (summarized in [8]) show that the propagation of the turbulent structures is dominated by the $\mathbf{E}_{rad} \times \mathbf{B}_{tor}$ shear and thus the v_{ph} well represents the poloidal plasma velocity.

Two statistical methods are exploited in order to estimate the v_{ph}: cross-correlation and cross-coherence techniques. The cross-correlation functions were calculated from the fluctuations of the U_{fl} or I_{sat} measured by poloidally spaced tips of the double rake probe. The sampling rate of the measured data and thus the temporal resolution of the cross-correlation function is 1 μs. The poloidal phase velocity of the turbulent structures v_{ph} is identified with ratio of mutual distance of the probes d over the time delay of the signal appearing successively at these two probes. The

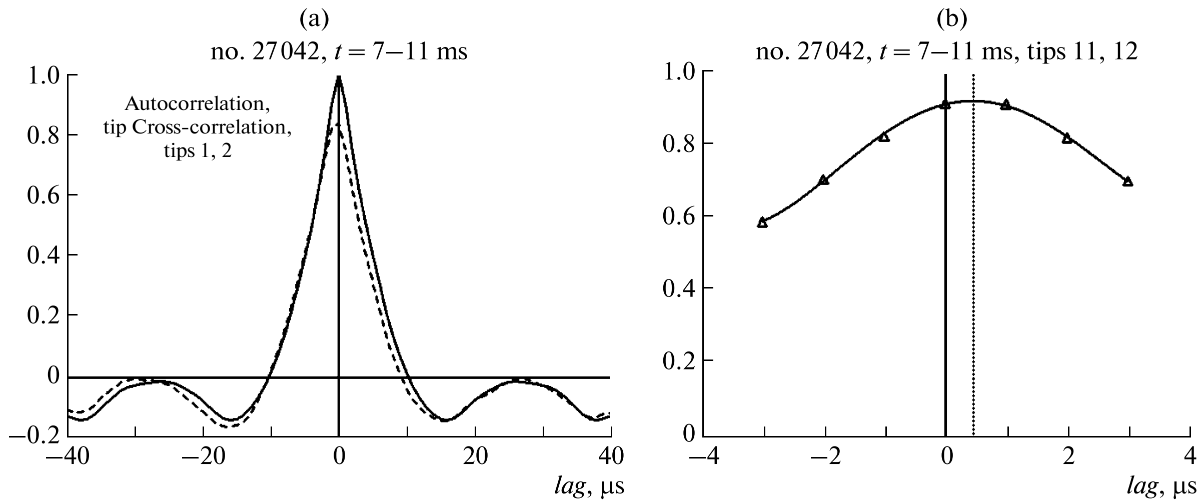

Fig. 4. (a) Auto-correlation (solid line) of a Langmuir probe and the cross-correlation (dashed line) of two adjacent probes as functions of lag; (b) detail of the cross-correlation function near the maximum of lag (triangles). The curve in plot (b) shows the polynomial fit near the lag_{max}. The dotted vertical line depicts the value of the lag_{max}. Shot no. 27042.

time the turbulent structures take to propagate from one probe to another was determined as the maximum time lag of the cross-correlation function of the two signals, lag_{max}. In order to improve the time resolution of this method above the limit imposed by the sampling period (1 μs) of the data acquisition system, the cross-correlation function is fitted by a polynom near its maximum. As a result, the phase velocity is calculated according to a simple relation [9]

$$v_{ph} = \frac{d}{lag_{max}}. \quad (1)$$

An example of the cross-correlation function and a detail of the polynomial fit are shown in Fig. 4.

Another method for evaluating the phase velocity is from the cross-coherence. The same tips were used for comparison of these two methods.

The phase velocity is calculated from the phase of the cross-coherence as [10]:

$$v_{ph} = \frac{2\pi d}{(\Delta\varphi/\Delta f)}, \quad (2)$$

where $\Delta\varphi/\Delta f$ is the derivative of the phase with respect to the frequency. The described process was performed for each poloidally spaced couple of tips. An example of the coherence and its phase spectrum is shown in Figs. 5a and 5b, respectively.

The resulting radial profiles of the poloidal phase velocity for U_{fl} (circles) and I_{sat} (triangles) fluctuations are shown in Fig. 6. The cross-correlation and cross-coherence methods showed the same values, thus they are not distinguished in the figure. It is evident that the sign of v_{ph} reverses at the radius of 70 mm corresponding to the LCFS (see Fig. 3).

The position of the velocity shear layer is established with a high precision in this experiment, as obvious from Fig. 6. The values of the velocity were compared to $\mathbf{E}_{rad} \times \mathbf{B}_{tor}$ drift estimation (solid curve). It is worth noting that a good agreement of the predicted velocity shear with the experimentally established one is observed when the electron part of the diamagnetic drift velocity $\mathbf{v}_{diam} = -\frac{\nabla p \times \mathbf{B}}{q n_e B^2}$ is added (v_{diam} is drawn by the dashed curve, and $v_{\mathbf{E}\times\mathbf{B}} + v_{diam}$, by the dotted one). For this phenomenon, we have no solid explanation.

In the proximity of the VSL, determination of the absolute values of the poloidal velocity using the cross-correlation and cross-coherence methods fails. The reason is omitting the radial velocity, which may cause serious overestimation of the poloidal phase velocity as will be described in following section.

The absolute values of v_{ph} from U_{fl} and I_{sat} are similar in the SOL, which means that the potential and the density structures are linked together. In the confinement area, however, the potential velocity seems to be higher. This is probably an artificial effect: the extent of the potential structures is larger than the density ones, thus the error (overestimation) of the method for evaluation v_{ph} is higher.

4. MODEL FOR CALCULATION OF v_{ph} OVERESTIMATION

In order to judge the error of the poloidal v_{ph} estimation introduced by the radial component of the phase velocity, a simple numerical model was devel-

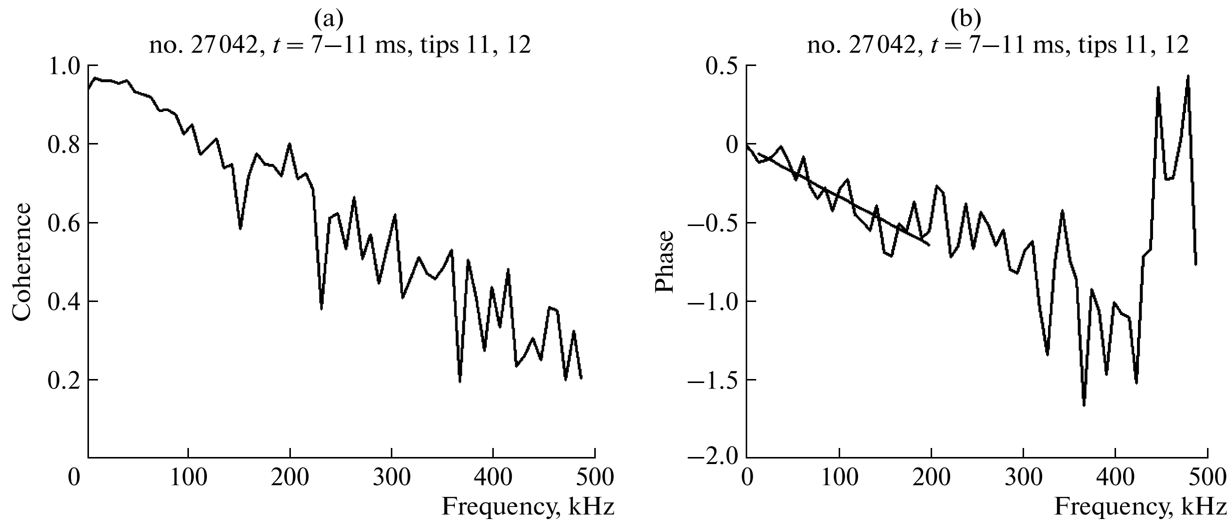

Fig. 5. (a) Cross-coherence and (b) phase spectrum of two adjacent probes. The line in plot (b) is a linear fit $\Delta\phi/\Delta f$ used for evaluation of the phase velocity according to formula (2). Shot no. 27042.

oped. A turbulent structure of Gaussian shape passing over the probe was considered:

$$A = \exp\left[-\left(\frac{r}{\Delta r}\right)^2 - \left(\frac{z}{\Delta z}\right)^2\right], \quad (3)$$

where A is the structure amplitude and

$$r = r_i - v_{rR}t, \quad z = z_i - v_{zR}t$$

are the structure's radial and poloidal positions, r_i and z_i are the radial and poloidal positions of the probe (i = 1, 2), and v_{rR} and v_{zR} are the radial and poloidal phase velocities. Then, $A_i(t)$ represents signal measured by the ith probe. Computing the cross-correlation function of $A_1(t)$ and $A_2(t)$ for the case of two probes separated purely poloidally by the distance of d, the time lag of the cross-correlation maximum $lag_{\max}$ can be expressed as

$$lag_{\max} = \frac{v_{zR}d}{v_{zR}^2 + \left(v_{rR}\frac{\Delta z}{\Delta r}\right)^2}. \quad (4)$$

Since this expression is independent on mutual position of the structure and of the pair of probes, structures with the same velocity but different poloidal shifts will all give the same time lag of the cross-correlation maximum. Then the ratio of the poloidal phase velocity v_{ph} established by the cross-correlation method (1) and the real poloidal phase velocity v_{zR} can be expressed as

$$\frac{v_{ph}}{v_{zR}} = 1 + \left(\frac{v_{rR}}{v_{zR}}\frac{\Delta z}{\Delta r}\right)^2, \quad (5)$$

where v_{rR} is the real radial phase velocity and Δr and Δz are the radial and poloidal extent of the structure, respectively.

Relation (5) implies that even a small contribution of the radial velocity may cause a significant over-estimation of v_{ph}. This effect is particularly visible in the proximity of the VSL where the radial velocity dominates the poloidal one. Extracting of the smaller radial

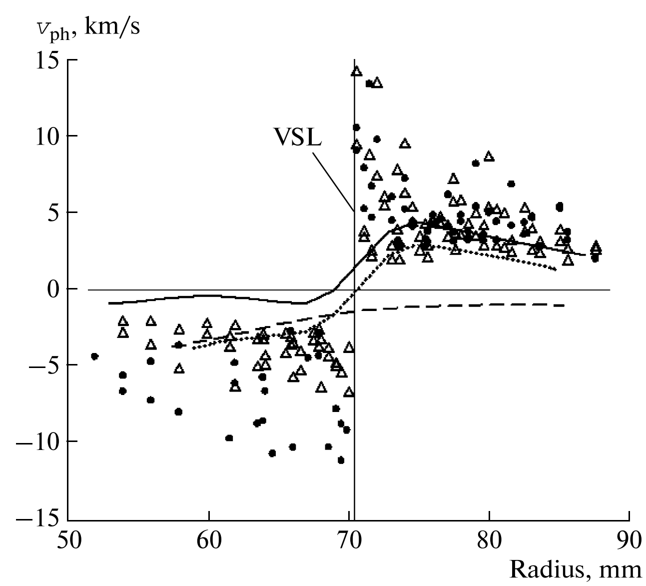

Fig. 6. Radial profile of the poloidal phase velocity of the turbulent structures. The circles stand for U_{fl}, and triangles for I_{sat}. The solid curve shows the $\mathbf{E}_{rad} \times \mathbf{B}_{tor}$ drift velocity; the dashed curve, the electron part of the diamagnetic drift velocity; and the dotted curve, the sum of these two. The vertical line depicts the VSL.

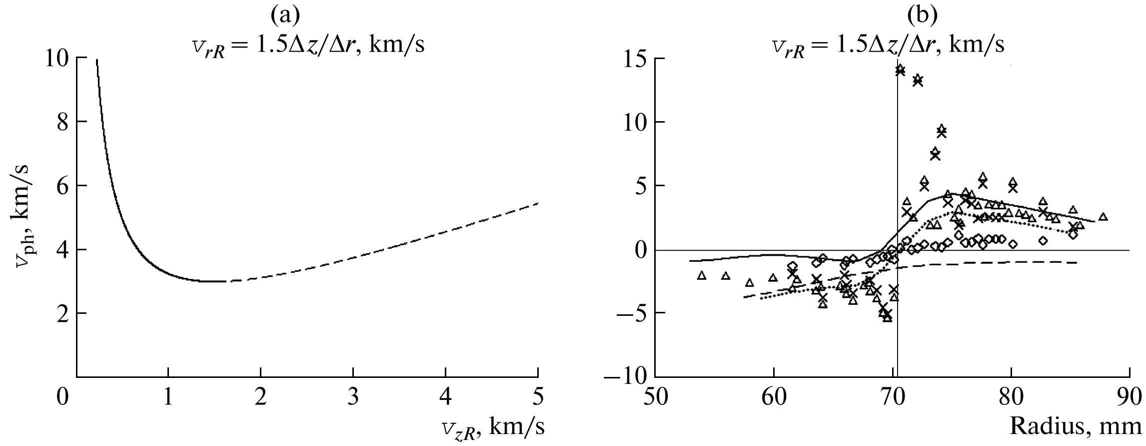

Fig. 7. (a) Phase velocity of plasma fluctuations v_{ph} as a function of v_{zR} calculated by formula (5) and (b) v_{ph} obtained experimentally from cross-correlations applied to I_{sat} data (triangles) and compared to the correction according to model (5): the crosses are for the high-velocity branch (the dashed curve in plot (a)), and the diamonds are for the low-velocity one (the solid curve in plot (a)).

component of the velocity is even more difficult than establishing the poloidal one because the radial phase velocity is usually smaller than the poloidal one.

In order to test the above mentioned hypothesis and to estimate the impact of the radial component of velocity on the calculation of the poloidal velocity, we have applied relation (5) to the experimental data. Figure 7a shows the dependence of the measured v_{ph} on the real poloidal velocity v_{zR}. This plot shows that one value of the poloidal velocity can result in two different estimations using the cross-correlations.

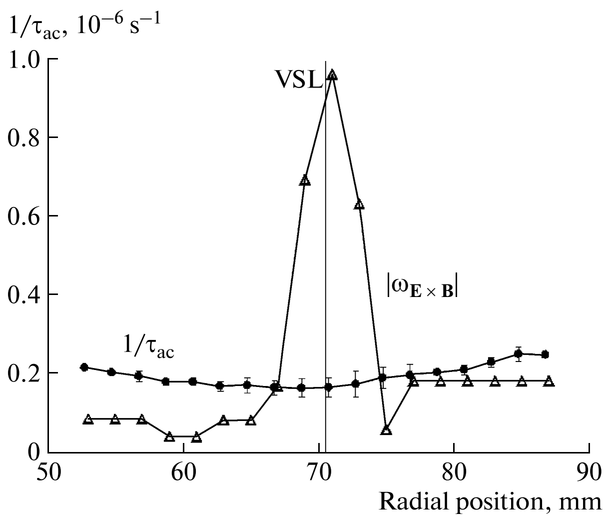

Fig. 8. Radial profile of $1/\tau_{ac}$ of the edge fluctuations (circles). The triangles shows the absolute value of the shearing rate $\omega_{\mathbf{E}\times\mathbf{B}}$. The vertical line depicts the VSL.

The real poloidal velocity v_{zR} was estimated by finding relevant values for each v_{ph} and plotted in Fig. 7b. The velocities were established from the ion saturation current; the floating potential gives a similar result. The triangles are the experimental v_{ph}, diamonds show the v_{zR} estimation coming from the low-velocity part of function (5) (the solid part of the curve in Fig. 7a), and the crosses show the v_{zR} from the high-velocity part (the dashed part of the curve). The three curves from Fig. 6 are over-plotted for illustration: solid for the $\mathbf{E}_{rad} \times \mathbf{B}_{tor}$ drift velocity, dashed for the electron part of the diamagnetic drift velocity, and dotted is the sum of these two. We have assumed a constant radial velocity, the factor $v_{rR}\dfrac{\Delta z}{\Delta r}$ was considered as equal to 1.5.

Figure 7a shows how the v_{ph} estimated from the cross-correlations is over-estimated. Near the VSL, the low-velocity branch is meaningful, while further, the experimental values as well as the estimations from the drifts agree with the high-velocity branch (the dashed part in Fig. 7a). The method has certain limitations, e.g., it assumes that all the structures have Gaussian shape, they are symmetric in radial and poloidal direction, and they have equal amplitudes, while in reality, they may be tilted and of different shape (short rising time and a long tail). Nevertheless, it is a nice illustration of limits of the method for evaluation of the velocity from Langmuir probes couples using cross-correlations.

Due to the above-mentioned reasons, we have a confidence in estimating the direction (sign) of the poloidal phase velocity, but the information on its absolute values is only qualitative.

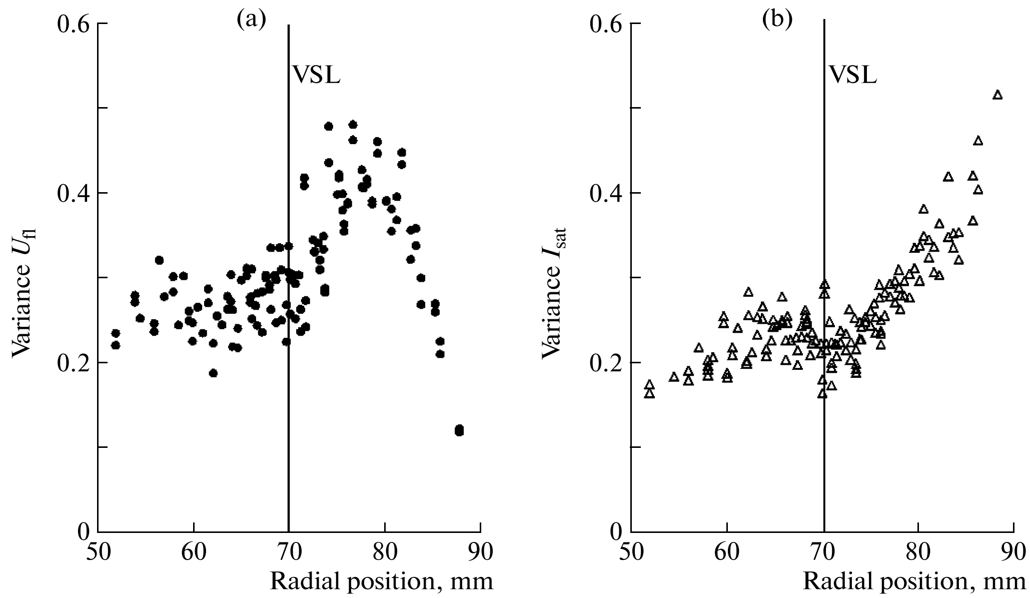

Fig. 9. (a) Radial profiles of the variance of U_{fl} (normalized to T_e) and (b) relative level of fluctuations I_{sat_fl}/I_{sat}.

5. TURBULENT STRUCTURES VERSUS VELOCITY SHEAR

It is widely recognized that the velocity shear has an impact on turbulent structures [11]. In order to estimate this effect, the shearing rate $\omega_{\mathbf{E}\times\mathbf{B}}$ has to be compared with the inverse of the correlation time of fluctuations $1/\tau_{ac}$. If $\omega_{\mathbf{E}\times\mathbf{B}} \approx 1/\tau_{ac}$, the system is in the state of marginal stability [3].

The maximum shearing rate $\omega_{\mathbf{E}\times\mathbf{B}}$ in the plasma edge of CASTOR can be estimated from the $\mathbf{E}_{rad} \times \mathbf{B}_{tor}$ drift as a radial derivation of the poloidal plasma velocity (the triangles in Fig. 6):

$$\omega_{\mathbf{E}\times\mathbf{B}} = \frac{dv_{pol}}{dr} \le 10^6\ \mathrm{s}^{-1}. \qquad (6)$$

The radial profile of $1/\tau_{ac}$ is shown in Fig. 8.

The shearing rate is comparable to $1/\tau_{ac}$ outside the VSL, as can be seen in Fig. 8. In the proximity of the VSL, the shearing rate is about five times higher than $1/\tau_{ac}$. Therefore, we can expect that the shear will dissipate the structures in this region.

Plotting of the statistical properties of the edge plasma signals can check the impact of the shear on the amplitude of fluctuations. The variance of the normalized U_{fl} to the T_e and the relative level of the density fluctuations (I_{sat_fl}/I_{sat}, where I_{sat_fl} is the fluctuation part of the ion saturation current and I_{sat} is its mean value) are plotted in Fig. 9. We can observe a local minimum in the relative level of density fluctuations near the VSL, which is a sign of a disturbance of the structures. This effect is not so apparent on the potential fluctuations.

6. CONCLUSIONS

Fluctuations of the ion saturation current (proportional to plasma density) and the floating potential (proportional to plasma potential) are measured with high spatial resolution at the edge of the CASTOR tokamak. The radial profile of the poloidal phase velocity of the turbulent structures is determined by two statistical methods. The radial position of the velocity shear layer where the poloidal rotation changes the sign is determined with high precision (~1 mm). The shearing rate is estimated in the proximity of the VSL as $\omega_{\mathbf{E}\times\mathbf{B}} \le 10^6\ \mathrm{s}^{-1}$ and found to be of the same values as the inverse of the correlation time of fluctuations $1/\tau_{ac}$ outside the VSL, but about five times higher in the proximity of the VSL.

In the VSL, a small reduction of the relative level is observed in the statistical parameters of the U_{fl} and I_{sat} signals. The system is in the state of marginal stability outside the VSL, while in the proximity of the VSL, the shear slightly dissipates the turbulent structures.

ACKNOWLEDGMENTS

This work was supported by the project AV0Z20430508 and by the Euratom Intra-European Fellowship EDGETURB.

REFERENCES

1. J. Wesson, *Tokamaks* (Clarendon, Oxford, 2004).
2. O. E. Garcia, N. H. Bian, V. Naulin, et al., Phys. Scr. **T122**, 104 (2006).
3. C. Hidalgo, B. Goncalves, M. A. Pedrosa, et al., J. Nucl. Mater. **313–316**, 863 (2003).
4. G. Van Oost, M. Berta, J. Brotankova, et al., Nucl. Fusion **47**, 378 (2007).
5. P. C. Stangeby, *The Plasma Boundary of Magnetic Fusion Devices* (IOP, Bristol, 2000).
6. J. Stockel, J. Adamek, P. Balan, et al., J. Phys., Conf. Series **63**, 012001 (2007).
7. R. Dejarnac, J. P. Gunn, J. Stockel, et al., Plasma Phys. Controlled Fusion **49**, 1791 (2007).
8. J. Schirmer, Nucl. Fusion **46**, S780 (2006).
9. G. Vayakis, PhD Thesis, University of Oxford, Oxford, 1991.
10. J. S. Bendat and A. G. Piersol, *Random Data: Analysis and Measurements Procedures* (Wiley, New York, 2000), p. 148.
11. P. Devynck, J. Brotankova, P. Peleman, et al., Phys. Plasmas **13**, 102505 (2006).